Bull. Mater. Sci. (2020) 43:45
https://doi.org/10.1007/s12034-019-1992-0

Synthesis, characterization and quantum chemical study of optoelectronic nature of ferrocene derivatives

AHMAD IRFAN[1,2,*], FIRAS KHALIL AL-ZEIDANEEN[3], ISHTIAQ AHMED[4], ABDULLAH G AL-SEHEMI[1], MOHAMMED A ASSIRI[1], SAMI ULLAH[1] and GHULAM ABBAS[3]

[1]Department of Chemistry, Faculty of Science, King Khalid University, P.O. Box 9004, Abha 61413, Saudi Arabia
[2]Research Center for Advanced Materials Science (RCAMS), King Khalid University, P.O. Box 9004, Abha 61413, Saudi Arabia
[3]Institut für Anorganische Chemie, Karlsruhe Institute of Technology, Engesserstrasse 15, 76131 Karlsruhe, Germany
[4]Institute for Biological Interfaces (IBG-1), Karlsruhe Institute of Technology (KIT), Hermann-von-Helmholtz-Platz, 76344 Eggenstein-Leopoldshafen, Germany
*Author for correspondence (irfaahmad@gmail.com)

MS received 15 May 2019; accepted 29 July 2019

Abstract. Two new ferrocene derivatives N-(2-hydroxy-5-methylphenyl) ferrocylideneamine (**Fe1**) and N-(2-hydroxy-5-chlorophenyl) ferrocylideneamine (**Fe2**) have been synthesized to study the effect on electronic, optical and charge transfer properties while changing the electron donating group with electron withdrawing group. The synthesized compounds were characterized by different spectroscopic (FTIR, UV–Vis, ^{1}H NMR, ^{13}C NMR) and spectrometric (EI) techniques. The geometries for ground and excited states were optimized by density functional theory (DFT/B3lyp/6-31G**, LANL2DZ) and time-dependent DFT (TD-B3lyp/6-31G**, LANL2DZ) levels, respectively. The absorption, fluorescence and phosphorescence spectra were estimated using TD-B3LYP and TD-wB97XD functionals and 6-31G** basis set for C, H, N, O and LANL2DZ for Fe atoms in dichloromethane.

Keywords. Semiconductors; ferrocenes; optoelectronic properties; charge transport; reorganization energy; frontier molecular orbitals.

1. Introduction

Conjugated transition metal complexes have gained immense interest due to their unique properties and potential applications in energy conversion, catalysis and semiconductor devices [1–7]. Ferrocene derivatives are gaining substantial consideration as smart thermochromic materials [8] as well as in optoelectronic devices due to thermal stability, decent solubility, flexibility towards synthesis of various new compounds and reversible redox nature because of the central iron atom [9,10]. Additionally, ferrocene derivatives [11–13] have applications, e.g., electronics [14], sensors [15], charge transport [16–18], biological treatments [19], catalysis and synthesis [20]. Ferrocenes are excellent electron donor materials owing to unique electrochemical and structural properties [21]. Moreover, they are being used in memory devices [22], nonlinear optics, organic field effect transistors (OFET), organic light-emitting diodes (OLEDs), etc. [23–25].

Previous studies showed that density functional theory (DFT) is an effective tool not only to reproduce the experimental evidences but also to reliably calculate numerous properties of interests [26,27]. The B3LYP functional [28–30] was effectively used to reproduce metal–carbon bond distance [31]. Previously, effective core potential (ECP) basis set method of Hay and Wadt (LanL2DZ) [32–35] was found to be consistent for ground state (S_0) geometry optimization [36]. Aliabad and Chahkandi [37] optimized the ferrocenes at B3LYP/LANL2DZ/6-311++g (d, p) level and later computed the band gaps by SPHYB and B3LYP functionals, which reproduced experimental evidence. Gryaznova *et al* [38] described the thermochemical properties and vibrational spectra of ferrocenes by BPW91, B3LYP and OPBE, and found B3LYP/6-31G*(LANL2DZ) level as rational. In another study by Francl *et al* [39], S_0 was optimized by LanL2DZ for Fe and 6-31G** for O, F, C, N, S and H.

The current work deals with the synthesis and characterization of two new ferrocene derivatives **Fe1** and **Fe2** (figure 1). To the best of our knowledge, there is no synthesis characterization, also, first-principle calculations of structural, electronic, optical and charge transfer (CT) properties of these two ferrocene derivatives have not been reported in literature. Thus, various properties of interests and the effect of electron donating group (EDG, $–CH_3$) and electron withdrawing group (EWG, –Cl) on the structural, electronic, optical and CT properties were investigated at molecular level.

Published online: 09 January 2020

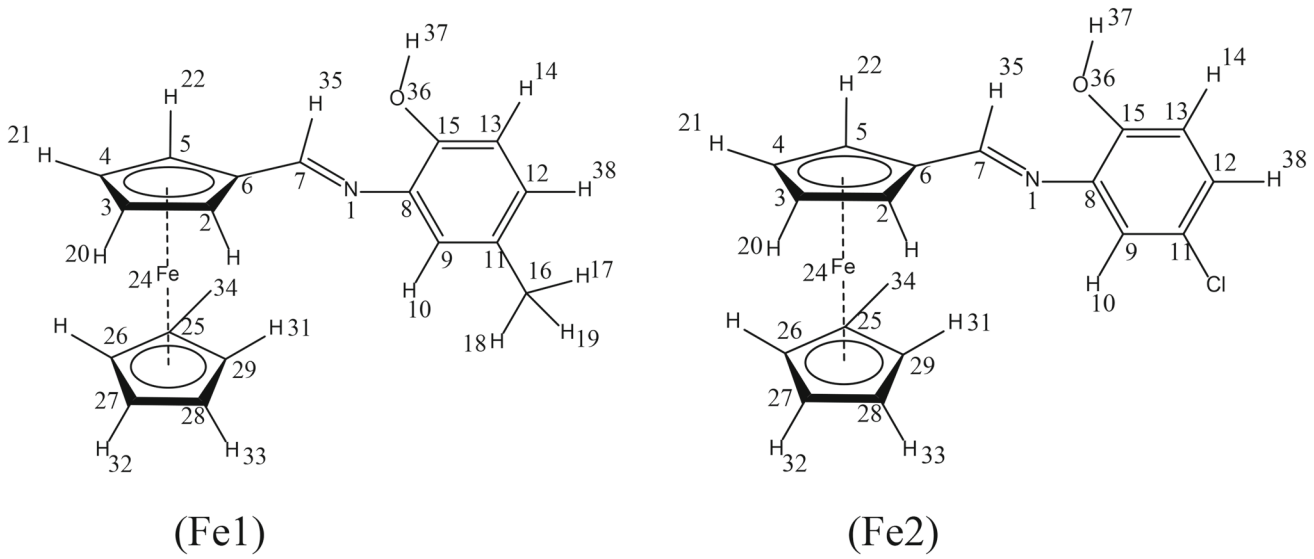

Figure 1. The structures of **Fe1** and **Fe2** (along with numbering scheme).

2. Methodology

2.1 *Experimental*

2.1a *Materials and methods*: Ferrocenecarboxaldehyde, 2-amino-4-chlorophenol and 2-amino-4-methylphenol were purchased from Acros Organics (Geel, Belgium). All the chemicals were of analytical grades and used as received. All reactions were carried out under aerobic conditions. The elemental analyses (C, H and N) were performed at the institute of inorganic chemistry (KIT) using an Elementar Vario EL analyser. Fourier transform IR spectra were measured on a Perkin-Elmer Spectrum One spectrometer with samples prepared as KBr discs. UV–Vis absorption spectroscopy of synthesized samples was carried out using a Varian Cary 500 Scan UV–Vis–NIR spectrophotometer. Solution NMR spectra were recorded using Bruker Avance instruments operating at ^{1}H Larmor frequency of 300 MHz, DMSO-d_6 as solvent and TMS as an internal standard for ^{13}C and ^{1}H nuclei.

2.1b *Synthesis of N-(2-hydroxy-5-methylphenyl) ferrocylideneamine (**Fe1**)*: Ferrocencarboxaldehyde (1.07 g, 5 mmol) and 2-amino-4-methylphenol (0.57 g, 5 mmol) were dissolved in 20 ml of ethanol (absolute) and the mixture was refluxed for 3 h. The reaction mixture was cooled down to room temperature and left overnight to afford brown precipitates. The product was purified by silica gel column chromatography using petroleum ether as solvent.

Yield: 55%. Calc. for **Fe1**: C, 67.73; H, 5.37; N, 4.39. Found: C, 67.43; H, 5.24; N, 4.21.

FT-IR (KBr cm^{-1}) 3103 (C–H str), 2921 (C–H str), 1619 (C=N str), 1104, 1106 (Ar–CH) 460.88, 497.99 cm^{-1} (Cp C–H). UV–Vis λ_{max} 355, 450.

^{1}H NMR (DMSO-d_6, 400 MHz) δ (ppm): 2.23 (s, 3H, CH_3), 4.26 (s, 5H, Fc-unsubstituted ring), 4.51 (s, 2H, H-3, H-4, Fc-substituted ring), 4.86 (s, 2H, H-2, H-5, Fc-substituted ring), 6.72 (d, J = 7.9 Hz, 1H, Ar–H), 6.81 (d, J = 7.9 Hz, 1H, Ar–H), 6.89 (s, 1H, Ar–H), 8.46 (s, 1H, CH=N).

^{13}C NMR (DMSO-d_6, 100 MHz) δ (ppm): 20.72 (CH_3), 69.34 (C-2, C-5, Fc-substituted ring), 69.58 (5C, Fc-unsubstituted ring), 71.38 (C-3, C-4, Fc-substituted ring), 81.33 (C-1, Fc-substituted ring), 115.88 (Ar–CH), 119.83 (Ar–CH), 126.97 (Ar–CH), 128.53 (Ar–C–CH_3), 139.09 (Ar–C–N), 148.35 (Ar–C–OH), 160.64 (CH=N).

MS (EI) m/z: 319.05 (mol. peak, 23.12%), 288.03 (7.61%), 254 (12.94%), 213.98 (100%), 185.99 (88.27%), 145.95 (1.45%), 128.04 (8.35%), 123.05 (24.97%), 122.04 (12.90%), 120.96 (81.01%), 93.94 (7.91%), 78.0 (7.12%), 65.02 (7.21%), 55.90 (38.48%).

2.1c *Synthesis of N-(2-hydroxy-5-chlorophenyl) ferrocylideneamine (**Fe2**)*: Ferrocencarboxaldehyde (1.07 g, 5 mmol) and 2-amino-4-chlorophenol (0.67 g, 5 mmol) were dissolved in a marginal quantity of ethanol (absolute) and the mixture was refluxed for 3 h. The reaction mixture was cooled down to room temperature and left overnight to obtain brown precipitates. The product was purified by column chromatography (SiO_2, petroleum ether).

Yield: 62%. Calc. for **Fe2**: C, 60.13; H, 4.16; N, 4.12. Found: C, 60.29; H, 4.05; N, 4.21.

FT-IR (KBr cm^{-1}) 3150 (C–H str), 3094 (C–H str), 1614 (C=N str), 1002.07, 999.78 (Ar–CH) 476.45, 499.1 cm^{-1} (Cp C–H). UV–Vis λ_{max} 353, 474.

^{1}H NMR (DMSO-d_6, 400 MHz) δ (ppm): 4.27 (s, 5H, Fc-unsubstituted ring), 4.54 (s, 2H, H-3, H-4, Fc-substituted ring), 4.86 (s, 2H, H-2, H-5, Fc-substituted ring), 6.84 (d, J = 8.3 Hz, 1H, Ar–H), 7.02 (d, J = 8.3 Hz, 1H, Ar–H),

7.10 (s, 1H, Ar–H), 8.49 (s, 1H, CH=N), 9.26 (bs, 1H, Ar–OH).

^{13}C NMR (DMSO-d_6, 100 MHz) δ (ppm): 69.58 (C-2, C-5, Fc-substituted ring), 69.70 (5C, Fc-unsubstituted ring), 71.68 (C-3, C-4, Fc-substituted ring), 80.78 (C-1, Fc-substituted ring), 117.47 (Ar–CH), 119.40 (Ar–CH), 123.30 (Ar–CH), 125.76 (Ar–C–Cl), 140.87 (Ar–C–N), 148.57 (Ar–C–OH), 162.85 (CH=N).

MS (EI) m/z: 339.0 (mol. peak, 35.86%, Cl^{35}), 340.99 (MP 11.45%, Cl^{37}), 273.95 (17.58%), 274.94 (5.98%), 213.98 (100%), 185.93 (85.05%), 142.99 (25.64%), 144.99 (8.23%), 128.04 (12.99%), 123.05 (24.97%), 122.04 (12.90%), 120.96 (88.18%), 93.94 (10.38%), 65.02 (11.83%), 55.90 (56.37%).

2.2 *Computational details*

Various quantum chemical approaches are very good tools not only to explain the properties of known materials but also to predict properties of interest of unexplored compounds. DFT [30,40–53] and time-dependent DFT (TDDFT) [54–56] are consistent methods used for the calculations of ground state (S_0) and excited state (S_1) properties. Hitherto, S_0 geometry optimizations of different compounds were computed using B3LYP functional along with ECP LANL2DZ for Ti [57]. In another study, it is shown that the geometries by B3LYP are in good agreement to MP2 with smaller computational cost [58]. The frequency calculations reveal that the optimized geometries are reliable, having no imaginary values representing an energy minimum. In the current work, the geometry optimizations were achieved using B3LYP functional and 6-31G** basis set for C, H, N, O, and LANL2DZ for Fe [59]. The frequency calculations coordinates revealed that the optimized geometries are reliable, having no imaginary values representing energy minima. It is recognized that B3LYP is insufficient for CT excitation calculations [60] due to self-interaction error, which underestimates the excitation energy [61,62]. It was reported that a long-range functional [63] would be a suitable choice for CT-type excitations [64]. The absorption (λ_a), fluorescence (λ_f) and phosphorescence (λ_{ph}) wavelengths were computed using TD-wB97XD and TD-B3LYP functionals of Self-Consistent Reaction Field (SCRF) in Polarizable Continuum Model (PCM) [65] in dichloromethane. The 6-31G** basis set was used for C, H, N, O and LANL2DZ for Fe.

Reorganization energy and polarization (λ) are significant parameters to evaluate CT rate [66]. The λ has two main components, i.e., internal/external polarization ($\lambda_{int}/\lambda_{ext}$) [67]. Here, λ_{int} was assessed for holes and electrons (λ_{hole} and λ_{elec}).

The λ_{hole} was calculated as $\lambda_1 + \lambda_2$ using equations (1 and 2) [68]:

$$\lambda_1 = E^+(\mathrm{Y}) - E^+(\mathrm{Y}^+) \quad (1)$$

$$\lambda_2 = E(\mathrm{Y}^+) - E(\mathrm{Y}) \quad (2)$$

where $E^+(\mathrm{Y})$, $E^+(\mathrm{Y}^+)$, $E(\mathrm{Y}^+)$ and $E(\mathrm{Y})$ are the energies of the cation in the optimized neutral structure, cation in the optimized cationic structure and neutral structure in the cationic state and optimized neutral state, respectively.

Similarly, λ_{elec} was calculated as $\lambda_3 + \lambda_4$ using equations (3 and 4):

$$\lambda_1 = E^-(\mathrm{Y}) - E^-(\mathrm{Y}^-) \quad (3)$$

$$\lambda_2 = E(\mathrm{Y}^-) - E(\mathrm{Y}) \quad (4)$$

where $E^-(\mathrm{Y})$ is the energy of anion in the optimized neutral state, $E^-(\mathrm{Y}^-)$ is the energy of the anion in optimized anionic state, $E(\mathrm{Y}^-)$ is the energy of the neutral structure in the anionic state and $E(\mathrm{Y})$ is the energy of the neutral structure in the optimized neutral state.

Formerly, B3LYP was found to be a sensible functional for the ionization potential (IP) calculations [69]. The vertical/adiabatic ionization potential (IP_v/IP_a), vertical/adiabatic electron affinity (EA_v/EA_a), λ_{hole} and λ_{elec} were computed at B3LYP/6-31G** (LANL2DZ) level. All the calculations were executed using Gaussian16 software [70].

3. Results and discussion

3.1 *UV–Vis analysis*

The electronic absorption spectra of ferrocene and substituted ferrocenes have been investigated intensely in the past. In ferrocene, the d_{z^2} orbital is the HOMO, centred on the metal, and a degenerate set of ligand orbitals in combination with the metal d_{xz} and d_{yz} is the LUMO. The absorptions around 450 and 474 nm in **Fe1** and **Fe2** are attributed to the $^1E_{1g} \rightarrow {}^1A_{1g}$ transition. A higher energy band around 355 and 353 nm has been assigned to the $^1E_{2g} \rightarrow {}^1A_{1g}$ transition, generally called as $\pi \rightarrow \pi^*$ transitions of the C=N group (see figure 2).

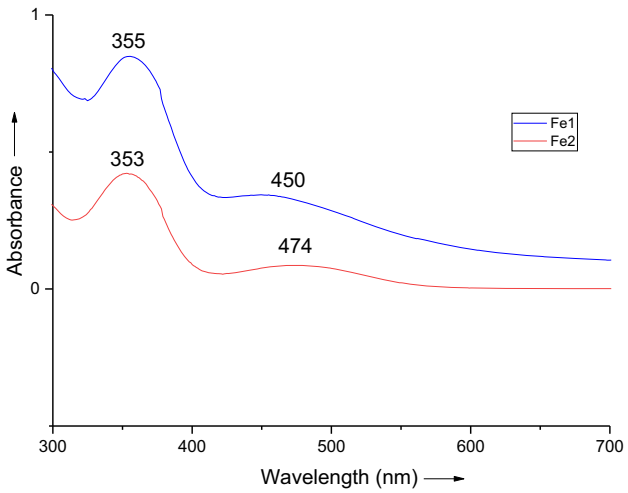

Figure 2. UV–Vis absorption spectra of compounds **Fe1** and **Fe2**.

3.2 *FR-IR and NMR studies*

The elemental analysis of the products is in good agreement with the calculated values. The structure of the compounds **Fe1** and **Fe2** was unambiguously confirmed by spectroscopic analysis. The IR spectra of the products show all the characteristic peaks. FT-IR spectra of **Fe1** and **Fe2** were recorded in the range of 4000–400 cm^{-1}. Imine function (C=N sp^2 stretching bands) of both compounds was registered as strong signals at 1619 and 1614 cm^{-1} in IR spectra, as well as at 8.46 and 8.49 ppm in ^{1}H NMR and at 160.64 and 162.85 ppm in ^{13}C NMR. The bands around 3103 cm^{-1} can be attributed to aromatic $^{\nu}$C−H. A band around 1104.27, 1106.03 cm^{-1} (**Fe1**) and 1002.07, 999.78 cm^{-1} (**Fe2**) due to ferrocene is observed in the spectra of the compounds. A Cp $^{\nu}$C–H stretching vibration is also seen around 460.88, 497.99 cm^{-1} (**Fe1**) and 476.45, 499.15 cm^{-1} (**Fe2**).

The hydrogen atoms of the unsubstituted cyclopentadienyl ring moiety appear as a sharp singlet, at 4.26 ppm for five hydrogens, and the substituted one at 4.51, 4.86 ppm for **Fe1** and for **Fe2**, substituted hydrogen at 4.27 ppm and substituted one at 4.54, 4.86 ppm. The aromatic C–H stretch in the ferrocene derivatives appeared at 2921 and 3094 cm^{-1} corresponding to C–H asymmetrical stretching vibration, and 3103, 3150 cm^{-1} for symmetrical stretching vibrations of **Fe1** and **Fe2**, respectively. Signals at 6.72, 6.81 and 6.89 ppm in ^{1}H NMR spectra of **Fe1** belong to phenyl protons. Phenyl carbon atoms in ^{13}C NMR gave the expected signals at 115.82, 119.83, 126.97, 128.53, 139.09 and 148.35 ppm, whereas the signal at 20.73 represents methyl-substituted carbon. Phenyl protons in **Fe2** give signals at 6.84, 7.02 and 7.10 ppm in ^{1}H NMR spectra, and in ^{13}C NMR this group gives signals at 117.47, 119.40, 123.30, 125.76 (Ar–C–Cl), 140.87 and 148.57 ppm. In the mass spectra of compounds **Fe1** and **Fe2**, peaks appearing at m/z 319.05 and 339.0 may be ascribed to $[L + H]^+$ and $[M - Cl]^+$, respectively.

3.3 *Geometries*

Certain optimized bond lengths and bond angle (ϕ) of **Fe1** and **Fe2** in their neutral, anionic and cationic forms are tabulated in table 1. The removal of the electron from HOMO increases the bond lengths of Fe–C6 and Fe–C29, i.e., 0.141 and 0.098 Å in **Fe1** and 0.132 and 0.099 Å in **Fe2** relative to the neutral form, respectively. Moreover, electron addition to LUMO also increases Fe–C6 bond length to 0.193 and 0.174 Å in **Fe1** and **Fe2** compared with the neutral form, respectively. Major alteration in ϕ from neutral to cationic forms was observed in C8–N1–C7, N1–C7–C6 and C6–Fe–C29, i.e., 2.63, −13.73 and 4.22° in **Fe1** and 3.47, −3.17 and 3.42° in **Fe2**, respectively. The main variation in ϕ from neutral to anionic forms was perceived in C9–C8–C15, C8–N1–C7, N1–C7–C6 and C2–C6–C5, i.e., −3.04, −3.40, −8.30 and −2.32° in **Fe1** and −2.18, −1.66, 1.49 and −2.54° in **Fe2**, respectively. It can be seen from table 1 that alteration in major geometrical parameters from neutral to cationic forms is greater than the neutral to anionic ones, which reveals that the greater polarization in previous case leads to increased hole reorganization energy than electron ones (details can be found in section 3.3).

Table 1. The optimized bond lengths (Å) and bond angles (ϕ, in degree) of ferrocene derivatives for the neutral (Y), cationic (Y^+) and anionic (Y^-) forms at ground states computed at B3LYP/6-31G**(LANL2DZ) level.

	Fe1					**Fe2**				
Parameter	Y	Y^+	Δ^a	Y^-	Δ^b	Y	Y^+	Δ^c	Y^-	Δ^d
N1–C7	1.278	1.292	0.014	1.328	0.050	1.285	1.290	0.005	1.331	0.046
N1–C8	1.407	1.385	−0.022	1.368	−0.039	1.400	1.388	−0.012	1.360	−0.04
C6–C7	1.468	1.456	−0.012	1.414	−0.054	1.457	1.459	0.002	1.415	−0.042
C8–C15	1.374	1.362	−0.012	1.433	0.059	1.419	1.424	0.005	1.436	0.017
C15–O35	1.412	1.423	0.011	1.377	−0.035	1.370	1.360	−0.010	1.375	0.005
C8–C9	1.399	1.415	0.016	1.420	0.021	1.405	1.413	0.008	1.428	0.023
C9–C11	1.403	1.389	−0.014	1.401	−0.002	1.390	1.385	−0.005	1.389	−0.001
Fe–C6	2.076	2.217	**0.141**	2.269	**0.193**	2.082	2.214	**0.132**	2.256	**0.174**
Fe–C29	2.077	2.175	**0.098**	2.126	0.049	2.080	2.179	**0.099**	2.119	0.039
C11–Cl	—	—		—		1.761	1.748	−0.013	1.790	0.029
C9–C8–C15	118.52	117.77	−0.75	115.48	**−3.04**	117.69	118.02	0.33	115.51	**−2.18**
C8–N1–C7	123.64	126.27	**2.63**	120.24	**−3.40**	122.75	126.22	**3.47**	121.09	−1.66
N1–C7–C6	131.82	118.05	**−13.77**	123.52	**−8.30**	121.21	118.04	**−3.17**	122.70	1.49
C2–C6–C5	107.03	106.92	−0.11	104.71	**−2.32**	107.42	107.06	−0.36	104.88	**−2.54**
C6–Fe–C29	108.23	112.45	**4.22**	109.90	1.67	109.28	112.70	**3.42**	109.70	0.42

$^{a/c}\Delta = \phi(Y) - \phi(Y^+)$; $^{b/d}\Delta = \phi(Y) - \phi(Y^-)$.

Bold values represent the 'significant change from neutral to ionic state or vice versa'.

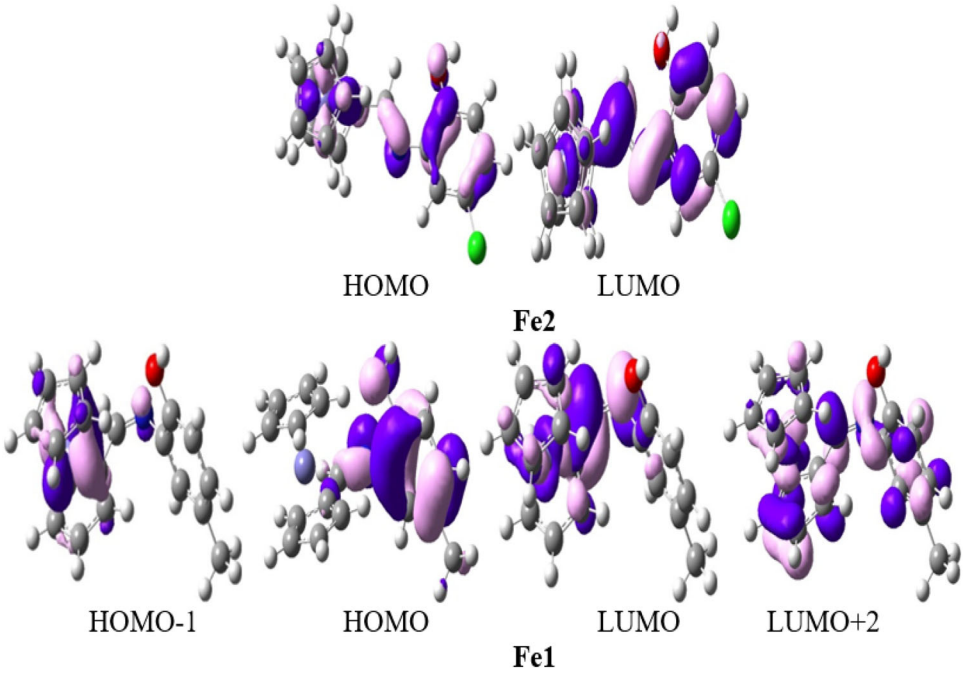

Figure 3. The ground state orbitals (0.035) involved in maximum absorption wavelength (transitions) at B3LYP/6-31G**(LANL2DZ).

3.4 *Electro-optical properties*

The S_0 and S_1 density plots of frontier molecular orbitals, i.e., highest occupied molecular orbitals (HOMO, HOMO−1, HOMO−2) and lowest unoccupied molecular orbitals (LUMO, LUMO + 2) involved in the major transition of absorption (λ_a) and fluorescence (λ_f) spectra of **Fe1** and **Fe2** are illustrated, respectively, in figures 3 and 4. At S_0, HOMO is delocalized on 2-hydroxy-5-methylphenyl moiety and HOMO–1 at Fe of ferrocene whereas LUMO is distributed at ferrocylideneamine unit and LUMO + 2 at the entire molecule in **Fe1**. In **Fe2** at S_0, HOMO and LUMO are on the entire molecule. At S_1, HOMO density is found on Fe of ferrocene, HOMO–2 at Fe of ferrocene as well as 2-hydroxy-5-chlorophenyl moiety whereas LUMO is distributed at ferrocylideneamine moiety in **Fe1**. In **Fe2** at S_1, the spatial distribution of HOMO and HOMO–2 is similar to that in **Fe1**, where LUMO is at the entire compound. At S_0, ligand–metal CT (LMCT) and metal–ligand CT (MLCT) were observed in **Fe1** with the transition H → L, H − 1 → L, H → L + 1 and H − 1 → L + 2, respectively. In **Fe2**, MLCT was perceived with the transition H → L. At S_1, LMCT was observed in **Fe1** with the transition L → H and MLCT with the transition L → H − 2. The LMCT was observed in **Fe2** with the transition L → H and intra-molecular CT (ICT) from phenyl moiety to –Cl and –OH substituents with the transition L → H − 2.

The computed HOMO energies (E_{HOMO}), LUMO energies (E_{LUMO}) and HOMO–LUMO energy gaps (E_{gap}) of S_0 and S_1 at the B3LYP/6-31G**(LANL2DZ) and TD-B3LYP/6-31G**(LANL2DZ) levels are tabulated in table 2, respectively. The substitution of –Cl (**Fe2**) on phenyl ring in place of $-CH_3$ (**Fe1**) has no substantial effect on the E_{HOMO} but it lowers the E_{LUMO}, resulting in reducing the E_{gap} in the previous compound.

The computed wavelengths for absorption (λ_a), fluorescence (λ_f) and phosphorescence (λ_{ph}) of ferrocene derivatives **Fe1** and **Fe2**, contribution of orbitals for computation [53], oscillator strengths (f) and major transitions at the TD-B3LYP/6-31G**(LANL2DZ) and TD-wB97XD/6-31G**(LANL2DZ) levels are tabulated in table 3. At S_0, transitions for λ_a were found in **Fe1** (H − 1 → L + 2, λ_a = 294 nm, f = 0.0354, H − 1 → L, λ_a = 251 nm, f = 0.1799) and in **Fe2** (H → L, λ_a = 333/301 nm, f = 0.4628/0.4876). At S_1, transitions for λ_f were found in **Fe1** (L → H − 2, λ_f = 373 nm, f = 0.0154, L → H, λ_f = 307 nm, f = 0.0377) and in **Fe2** L → H − 2, λ_f = 349 nm, f = 0.4455, L → H, λ_f = 310 nm, f = 0.600) at TD-B3LYP/6-31G**(LANL2DZ) and TD-wB97XD/6-31G**(LANL2DZ) levels, respectively.

The –Cl substitution replacing $-CH_3$ led to red-shift in λ_a. The f also increased on introducing EWG –Cl. The λ_f and λ_{ph} are blue-shifted on introducing –Cl in place of $-CH_3$ at TD-B3LYP/6-31G**(LANL2DZ) level while being red-shifted at TD-wB97XD/6-31G**(LANL2DZ) level.

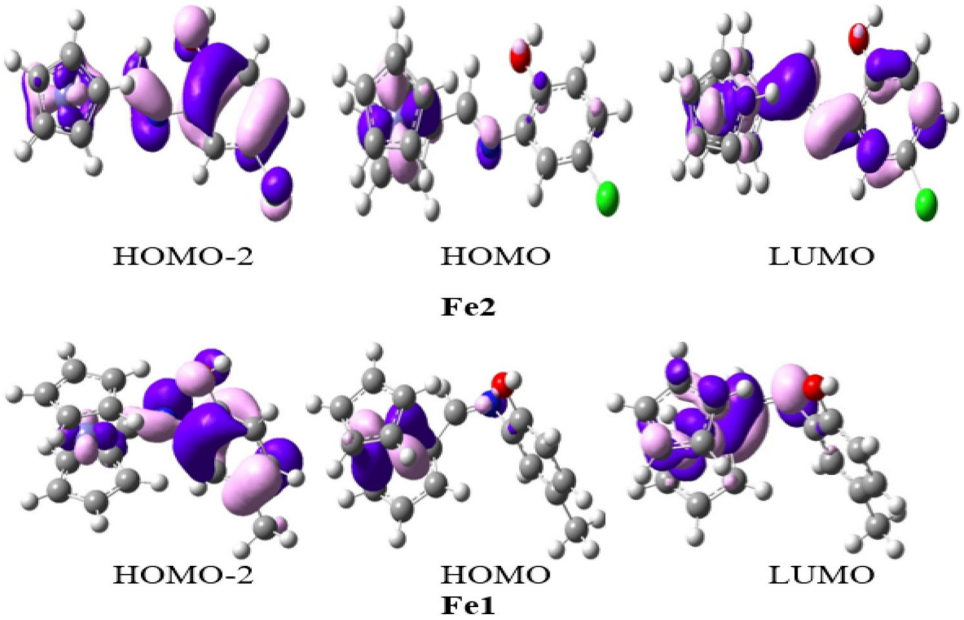

Figure 4. The excited state orbitals (0.035) involved in maximum fluorescence wavelength (transitions) at TD-B3LYP/6-31G**(LANL2DZ) level.

Table 2. The calculated ground (S_0) and excited (S_1) states HOMO energies (E_{HOMO}), LUMO energies (E_{LUMO}) and HOMO–LUMO energy gaps (E_{gap}) in eV at the B3LYP/6-31G**(LANL2DZ) and TD-B3LYP/6-31G**(LANL2DZ) levels, respectively.

	S_0			S_1		
Compounds	E_{HOMO}	E_{LUMO}	E_{gap}	E_{HOMO}	E_{LUMO}	E_{gap}
Fe1	−5.34	−0.86	4.48	−5.29	−1.25	4.04
Fe2	−5.47	−1.32	4.15	−5.26	−1.53	3.73

Table 3. The calculated absorption (λ_a), fluorescence (λ_f) and phosphorescence (λ_{ph}) wavelengths in nm of ferrocene derivatives, their oscillator strengths (f) and major transitions at the TD-B3LYP/6-31G**(LANL2DZ) and TD-wB97XD/6-31G**(LANL2DZ) levels, respectively.

Compounds	λ_a	f	Transition	λ_f	f	Transition	λ_{ph}	Transition
Fe1	294	0.0354	H − 1 → L + 2	373	0.0154	L → H − 2	415	L → H − 2
	(251)	(0.1799)	H − 1 → L	(307)	(0.0377)	L → H	(368)	L → H
Fe2	333	0.4628	H → L	349	0.4455	L → H − 2	381	L + 2 → H − 1
	(301)	(0.4876)	H → L	(310)	(0.600)	L → H	(455)	L → H

Values in parentheses are at TD-wB97XD/6-31G**(LANL2DZ).

3.5 *CT properties*

The calculated λ_{hole}, λ_{elec} and total internal reorganization energies (λ_{int}) along with their components λ_1−λ_4 for **Fe1** and **Fe2** at the B3LYP/6-31G**(LANL2DZ) level are tabulated in table 4. The λ_{hole} are larger than λ_{elec} with the difference ($\Delta\lambda$) of 0.456 and 0.351 eV for **Fe1** and **Fe**, respectively. Earlier, it was shown that smaller λ values would lead to improved CT rate [48,71]. Replacing $-CH_3$ by –Cl causes less structural alteration (less polarization) from neutral to anion states, leading to smaller λ_{elec} values.

The λ_{elec} values are significantly smaller than the λ_{hole} for **Fe1** and **Fe2**, from which it can be anticipated that these ferrocene derivatives may be better electron transfer materials. Heretofore, it was established that larger EA

Table 4. The calculated vertical/adiabatic ionization potential (IP_v/IP_a), vertical/adiabatic electron affinity (EA_v/EA_a), hole reorganization energies (λ_{hole}), electron reorganization energies (λ_{elec}) and total internal reorganization energies (λ_{int}) along with their components $\lambda_1-\lambda_4$ calculated at the B3LYP/6-31G**(LANL2DZ) level.

Compounds	IP_a	EA_a	IP_v	EA_v	λ_1	λ_2	λ_{hole}	λ_3	λ_4	λ_{elec}	$\Delta\lambda^a$
Fe1	5.766	0.298	7.115	−0.362	0.0113	1.348	1.359	0.242	0.660	0.903	0.456
Fe2	6.072	0.406	7.048	0.007	0.159	0.976	1.135	0.382	0.399	0.781	0.354

[a] $\Delta\lambda =$ difference between λ_{hole} and λ_{elec}.

would encourage better electron transport. The larger EA and smaller λ_{elec} values for **Fe2** than **Fe1** show that the previous compound might be a better electron transport material.

4. Conclusions

The removal of the electron from HOMO or electron addition to LUMO increases the bond lengths of Fe–C6 and Fe–C29 relative to the neutral form. At ground state, LMCT and MLCT were observed in **Fe1** with the transition H $\rightarrow$ L, H $\rightarrow$ L + 1 and H − 2 $\rightarrow$ L + 2, respectively. In **Fe2**, MLCT was perceived with the transition H $\rightarrow$ L. At excited state, LMCT was observed in **Fe1** with the transition L $\rightarrow$ H and MLCT with the transition L $\rightarrow$ H − 2. The LMCT was observed in **Fe2** with the transition L $\rightarrow$ H and intra-molecular charge transfer (ICT) from phenyl moiety to –Cl and –OH substituents with the transition L $\rightarrow$ H − 2. The substitution of –Cl (**Fe2**) on phenyl ring in place of $-CH_3$ (**Fe1**) has no significant effect on the E_{HOMO} but it lowers the E_{LUMO}, resulting in reducing the E_{gap} in the previous compound. The –Cl substitution in place of $-CH_3$ led to red-shift in absorption, fluorescence and phosphorescence spectra at TD-wB97XD/6-31G**(LANL2DZ) level. The –Cl in place of $-CH_3$ leads to less structural alteration (less polarization) from neutral to anion states, leading to smaller λ_{elec} values. The alteration in major geometrical parameters from neutral to anionic forms is less than the neutral to cationic ones, which shows that the smaller polarization in previous case leads to decreased λ_{elec}, resulting in enhanced electron transportability. The larger electron affinity and smaller λ_{elec} values for **Fe2** than **Fe1** show that the previous compound may be a better electron transport material. These results reveal that these ferrocene derivatives can be used in semiconductor and optoelectronic devices.

Acknowledgements

We extend our appreciation to the Deanship of Scientific Research at King Khalid University (KKU) for funding this work through research groups program under grant number R.G.P.2/15/40.

References

[1] Ovchenkova E N, Bichan N G and Lomova T N 2018 *Russ. J. Inorg. Chem.* **63** 391
[2] Nishihara H 1997 in *Handbook of organic conductive molecules and polymers* H S Nalwa (ed), Chapter 19, vol. 2 (Weinheim: Wiley) p 799
[3] Long X, Qiu W, Wang Z, Wang Y and Yang S 2019 *Mater. Today Chem.* **11** 16
[4] Khan M D, Malik M A and Revaprasadu N 2019 *Coord. Chem. Rev.* **388** 24
[5] Abbas G, Hassan A, Irfan A, Mir M and Wu G 2015 *J. Struct. Chem.* **56** 92
[6] Ghosh N N, Habib M, Pramanik A, Sarkar P and Pal S 2018 *Bull. Mater. Sci.* **41** 56
[7] Arunkumar A, Prakasam M and Anbarasan P M 2017 *Bull. Mater. Sci.* **40** 1389
[8] Wang S, Xu Z, Wang T, Xiao T, Hu X Y, Shen Y Z *et al* 2018 *Nat. Commun.* **9** 1737
[9] Bishop J J, Davison A, Katcher M L, Lichtenberg D W, Merrill R E and Smart J C 1971 *J. Organomet. Chem.* **27** 241
[10] Nerngchamnong N, Yuan L, Qi D C, Li J, Thompson D and Nijhuis C A 2013 *Nat. Nanotechnol.* **8** 113
[11] Inkpen M S, Scheerer S, Linseis M, White A J P, Winter R F, Albrecht T *et al* 2016 *Nat. Chem.* **8** 825
[12] Astruc D 2017 *Europ. J. Inorg. Chem.* **2017** 6
[13] Larik F A, Saeed A, Fattah T A, Muqadar U and Channar P A 2017 *Appl. Organomet. Chem.* **31** e3664
[14] Morari C, Rungger I, Rocha A R, Sanvito S, Melinte S and Rignanese G M 2009 *ACS Nano* **3** 4137
[15] Radhakrishnan S and Paul S 2007 *Sens. Actuator B: Chem.* **125** 60
[16] Zhu Y, Clot O, Wolf M O and Yap G P A 1998 *J. Am. Chem. Soc.* **120** 1812
[17] Templeton A C, Wuelfing W P and Murray R W 2000 *Acc. Chem. Res.* **33** 27
[18] Getautis V, Daskeviciene M, Malinauskas T and Jankauskas V 2007 *Monatsh. Chem.* **138** 277
[19] Shago R F, Swarts J C, Kreft E and Van Rensburg C E J 2007 *Anticancer Res.* **27** 3431
[20] Togni A and Hayashi T 1995 *Ferrocenes: homogeneous catalysis, organic synthesis, materials science* (Weinheim: Wiley-VCH) ISBN 3-527-29048-6
[21] Imahori H, Norieda H, Yamada H, Nishimura Y, Yamazaki I, Sakata Y *et al* 2001 *J. Am. Chem. Soc.* **123** 100
[22] Zhang B, Fan F, Xue W, Liu G, Fu Y, Zhuang X *et al* 2019 *Nat. Commun.* **10** 736
[23] Tan H, Yao H, Song Y, Zhu S, Yu H and Guan S 2017 *Dyes Pigm.* **146** 210

[24] Kanthasamy K, Ring M, Nettelroth D, Tegenkamp C, Butenschön H, Pauly F *et al* 2016 *Small* **12** 4849
[25] Singla P, Van Steerteghem N, Kaur N, Ashar A Z, Kaur P, Clays K *et al* 2017 *J. Mater. Chem. C* **5** 697
[26] Orendt A M, Facelli J C, Jiang Y J and Grant D M 1998 *J. Phys. Chem. A* **102** 7692
[27] Mayor-López M J and Weber J 1997 *Chem. Phys. Lett.* **281** 226
[28] Hohenberg P and Kohn W 1964 *Phys. Rev.* **136** B864
[29] Kohn W, Becke A D and Parr R G 1996 *J. Phys. Chem.* **100** 12974
[30] Lee C, Yang W and Parr R G 1988 *Phys. Rev. B* **37** 785
[31] Coriani S, Haaland A, Helgaker T and Jørgensen P 2006 *Chem. Phys. Chem.* **7** 245
[32] Hay P J and Wadt W R 1985 *J. Chem. Phys.* **82** 270
[33] Wadt W R and Hay P J 1985 *J. Chem. Phys.* **82** 284
[34] Hay P J and Wadt W R 1985 *J. Chem. Phys.* **82** 299
[35] Irfan A, Chaudhry A R, Jin R, Al-Sehemi A G, Muhammad S and Tang S 2017 *J. Taiwan Inst. Chem. Eng.* **80** 239
[36] Irfan A and Abbas G 2018 *Z. Naturforsch. A* **73** 337
[37] Aliabad H A R and Chahkandi M 2017 *Z. Anorg. Allg. Chem.* **643** 420
[38] Gryaznova T P, Katsyuba S A, Milyukov V A and Sinyashin O G 2010 *J. Organomet. Chem.* **695** 2586
[39] Francl M M, Pietro W J, Hehre W J, Binkley J S, Gordon M S, DeFrees D J *et al* 1982 *J. Chem. Phys.* **77** 3654
[40] Becke A D 1993 *J. Chem. Phys.* **98** 5648
[41] Irfan A and Mahmood A 2018 *J. Clust. Sci.* **29** 359
[42] Irfan A, Assiri M and Al-Sehemi A G 2018 *Org. Electron.* **57** 211
[43] Irfan A, Chaudhry A R, Muhammad S and Al-Sehemi A G 2019 *Optik* **179** 526
[44] Irfan A, Al-Sehemi A G, Chaudhry A R, Muhammad S and Asiri A M 2016 *Optik* **127** 10148
[45] Irfan A 2014 *Optik* **125** 4825
[46] Reeta Felscia U, Rajkumar B J M and Briget Mary M 2018 *J. Mater. Sci.* **53** 15213
[47] Yang G, Su Z and Qin C 2006 *J. Phys. Chem. A* **110** 4817
[48] Wazzan N, El-Shishtawy R M and Irfan A 2017 *Theor. Chem. Acc.* **137** 9
[49] Wazzan N and Irfan A 2018 *Org. Electron.* **63** 328
[50] Irfan A 2019 *Comput. Theor. Chem.* **1159** 1
[51] Irfan A 2019 *Results Phys.* **13** 102304
[52] Irfan A, Al-Sehemi A G, Assiri M A and Mumtaz M W 2019 *Bull. Mater. Sci.* **42** 145
[53] Pratik S M and Datta A 2013 *Phys. Chem. Chem. Phys.* **15** 18471
[54] Akhtaruzzaman M, Seya Y, Asao N, Islam A, Kwon E, El-Shafei A *et al* 2012 *J. Mater. Chem.* **22** 10771
[55] Chen J, Bai F Q, Wang J, Hao L, Xie Z F, Pan Q J *et al* 2012 *Dyes Pigm.* **94** 459
[56] Fan W, Tan D and Deng W Q 2012 *Chem. Phys. Chem.* **13** 2051
[57] Zhang J, Li H B, Sun S L, Geng Y, Wu Y and Su Z M 2012 *J. Mater. Chem.* **22** 568
[58] Preat J, Michaux C, Jacquemin D and Perpète E A 2009 *J. Phys. Chem. C* **113** 16821
[59] Irfan A, Jin R, Al-Sehemi A G and Asiri A M 2013 *Spectrochim. Acta A* **110** 60
[60] Dev P, Agrawal S and English N J 2013 *J. Phys. Chem. A* **117** 2114
[61] Autschbach J 2009 *Chem. Phys. Chem.* **10** 1757
[62] Dreuw A and Head-Gordon M 2005 *Chem. Rev.* **105** 4009
[63] Yanai T, Tew D P and Handy N C 2004 *Chem. Phys. Lett.* **393** 51
[64] Pastore M, Mosconi E, De Angelis F and Grätzel M 2010 *J. Phys. Chem. C* **114** 7205
[65] Takano Y and Houk K N 2005 *J. Chem. Theory Comput.* **1** 70
[66] Bhattacharyya K and Datta A 2017 *J. Phys. Chem. C* **121** 1412
[67] Brédas J L, Beljonne D, Coropceanu V and Cornil J 2004 *Chem. Rev.* **104** 4971
[68] Zhao C, Wang W and Ma Y 2013 *Comput. Theor. Chem.* **1010** 25
[69] Li P, Bu Y and Ai H 2004 *J. Phys. Chem. A* **108** 1200
[70] Frisch M J, Trucks G W, Schlegel H B, Scuseria G E, Robb M A, Cheeseman J R *et al* 2016 Gaussian16 software (Wallingford, CT: Gaussian, Inc.)
[71] Chai W and Jin R 2016 *J. Mol. Struct.* **1103** 177